Ultrasonic detection based on polarization-dependent optical reflection

Article *in* Optics Letters · February 2017

DOI: 10.1364/OL.42.000439

Optics Letters

Ultrasonic detection based on polarization-dependent optical reflection

Xiaoyi Zhu, Zhiyu Huang, Guohe Wang, Wenzhao Li, Da Zou, and Changhui Li*

Department of Biomedical Engineering, College of Engineering, Peking University, Beijing 100871, China

**Corresponding author: chli@pku.edu.cn*

Received 17 October 2016; revised 14 December 2016; accepted 16 December 2016; posted 19 December 2016 (Doc. ID 278671); published 19 January 2017

Owing to their extremely wide bandwidths, pure optical ultrasonic detection methods are gaining increasing interest. In this Letter, we proposed a simple ultrasonic detector that is based on the polarization-dependent optical reflection. When the acoustic wave reaches the liquid-glass interface, the acoustic pressure changed the relative refractive index between two media, leading to perturbations in the reflectance of the optical probe beam in glass. Unlike previous studies that detected the modulations in the intensity of the reflected beam, our method, named "polarization-dependent reflection ultrasonic detection (PRUD)," detects the intensity difference between two polarization components of the same probe beam. The PRUD significantly increased the sensitivity. Besides a phantom study, we also successfully detect weak photoacoustic waves in an *in vivo* animal experiment. This novel method can provide a simple way for ultrasonic detection, which will have great potential for ultrasound and photoacoustic imaging and sensing.

OCIS codes: (170.0110) Imaging systems; (170.5120) Photoacoustic imaging; (110.7170) Ultrasound; (130.6010) Sensors.

https://doi.org/10.1364/OL.42.000439

Ultrasonic detectors with broadbands, small sizes, and high sensitivity are desired for both ultrasound imaging and the emerging photoacoustic tomography (PAT). It is particularly valuable for PAT since the large-scale differences in various optical absorbers could lead to extremely wide bandwidth photoacoustic pressure waves [1–4]. Although various kinds of piezoelectric-material-based ultrasound transducers have been commercially available and widely used, these transducers generally have limited bandwidths (centered at their resonant frequency), and the electrical noise significantly increases as the transducer becomes smaller. Due to their high sensitivity, superior wide bandwidths, small effective active sizes, as well as other good characteristics, several pure optical ultrasonic detection methods have been developed, including the Mach–Zehnder interferometer [5], the surface displacement interferometer [6], full-field speckle interferometry [7], the Fabry–Perot polymer [8], the microring resonator [9,10], the low-coherence interferometer [11], and the surface plasmon resonance detector [12].

Among these pure optical methods, one of the simplest is based on the modulations of light reflectivity at an interface due to the refractive index variations caused by the ultrasonic pressure [13,14]. A typical setup of this method was presented in Fig. 1. The optical power incident on the interface is P_0 and the reflected power is $R_{\text{opt}}P_0$, where R_{opt} represents the reflectivity.

According to the Fresnel's reflection law, the optical intensity reflectivity on the interface can be derived as

$$R_s = \left[\frac{\sin(r_w - r_g)}{\sin(r_w + r_g)}\right]^2, \qquad R_p = \left[\frac{\tan(r_g - r_w)}{\tan(r_g + r_w)}\right]^2, \tag{1}$$

where R_s and R_p represent the optical intensity reflectivity of a p-wave and an s-wave, respectively, and the reflectivity for unpolarized light is $R_{\text{opt}} = (R_s + R_p)/2$; r_g and r_w are angles between the incident beam and the refraction beam with the normal of the interface, respectively. The angles are related according to Snell's law:

$$n_g \sin r_g = n_w \sin r_w, \tag{2}$$

where n_g and n_w represent the refractive indices of the glass prism and water, respectively. Although the acoustic pressure can change both n_g and n_w, the contribution to the reflectivity modulation from n_g is much smaller than that from n_w, as discussed in [15]. Therefore, only n_w close to the interface was considered in this Letter. According to the previous literature, the influence of the pressure on n_w is

$$dn_w/dn_p = 1.35 \times 10^{-10}\ \text{Pa}^{-1}. \tag{3}$$

Because of the laser instability, spontaneously environmental variation (dust, mechanical vibration, etc.), as well as the electrical noise background from the detector, the minimum pressure

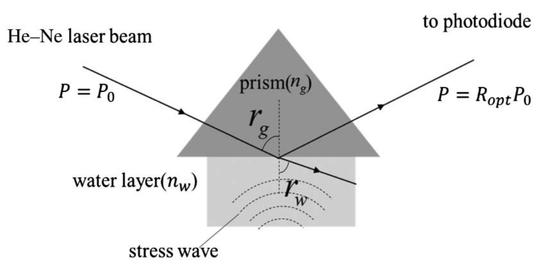

Fig. 1. Typical ultrasonic detector based on the reflectivity of the light on the interface.

it can detect is in the order of 1 bar. It is enough to detect strong shock waves, but it is not suitable for *in vivo* biomedical imaging purposes. Inspired by the reported graphene-based optical detector that used the polarization dependence reflectance [16], in this Letter, we proposed the "polarization-dependent reflection ultrasonic detection" (PRUD). The PRUD does not require any coating on the detection surface. Our current PRUD shows good linear response to acoustic pressure over the range of 500 Pa ~48 kPa and achieves ultrabroad frequency response from almost zero to 137.2 MHz (–6 dB). Therefore, with orders of improvement in the minimum detected pressure, PRUD make it very promising for *in vivo* studies.

The mechanism of PRUD is based on detection of the polarization dependence reflectance, i.e., the reflectance difference between the p-wave and the s-wave, as shown in Fig. 2(a). To achieve the best performance of the balanced detection, the p-wave and the s-wave have almost the same intensity, and the small difference in the reflectivity ($\Delta R = R_s - R_p$) was amplified.

The ΔR is also a function of both the refractive index and incident angles. In our design, we initially encoded the probe beam to be circularly polarized, and separated the reflected beam into a p-wave and an s-wave by a polarization beam splitter (PBS). Then, the two components were detected by a balance amplified photodetector. Because the p-wave and the s-wave components travel most of the same route before reaching the detector, the common mode rejection mechanism in the balanced detector can effectively suppress much of the unwanted signals that originated from laser instability and environmental variations, which is crucial to detect weak signal from the strong background. We can calculate the sensitivity of this detector as a derivative of ΔR and the pressure

$$S = \frac{d\Delta R}{dp}. \quad (4)$$

Figure 2(b) shows the dependence of the sensitivity S on the incident angle r_g at $p = 0$. The sensitivity rises sharply as r_g approaches the critical angle of total internal reflection ($n_g = 1.4570187$ and $n_w = 1.334$. The critical angle is calculated to be $r_{0,g} = 66.2865°$).

We developed a PRUD system, as shown in Fig. 3; the design is inspired by [12]. The material of PRUD head is a trapezoid prism made of fused silica. A continuous He–Ne laser (25-LHP-991-230, Melles Griot; wavelength, 632.8 nm; power, 9 mW; mode, >90%TEM$_{00}$; beam diameter, ~1.02 mm) was used as the probe beam. After passing through a neutral density filter, the probe laser is tuned to be circularly polarized by a polarizer (LPVISB100, Thorlabs) and a quarter-wave plate (WPQ05M-633, Thorlabs). Then, it is weakly focused through a convex lens onto the bottom surface of the trapezoid prism. The size of the spot (effective detector size) on the interface is about 200 × 100 μm. The reflected probe beam is then focused by another convex lens, separated by a polarization beam splitter (PBS201, Thorlabs) into a p-wave and an s-wave, and detected by a high-frequency balanced detector (PDB450A, Thorlabs). Since the system sensitivity is highly sensitive to the incident angle when close to the critical angle, we mounted the trapezoid prism on a high-precision rotational stage (WN01RM73, Winner Optical Instruments Group Company Ltd.) to perform fine-tuning of the incident angle.

To test the bandwidth of the system, we excited a 100 nm thick graphene film that coated on a glass sheet to generate a broadband PA signal, as shown in Fig. 2(a). The glass plate was placed under the prism, and a thin layer of deionized (DI) water was filled with the gap between the glass plate and the prism as the coupling medium. The excitation light is a 532 nm Nd:YAG pulsed laser (Elforlight SPOT-10-100-532; pulse width < 1.8 ns; pulse energy, 3.8 μJ; mode, TEM$_{00}$, M^2<1.1; beam diameter, ~1 mm), which passed downward through the transparent trapezoid prism and illuminated on the graphene film. A signal from the balanced amplify detector was filtered through a 150 MHz low-pass filter (Mini-Circuits, BLP-150+; DC-140 MHz) and recorded by a digital oscilloscope (DPO 3034, Tektronix). Figure 4(a) shows the frequency spectrum of the recorded signal. The detection bandwidth of the PRUD is calculated to be 137.2 MHz at –6 dB, and it shows a relatively flat frequency response over a wide range.

To quantify the sensitivity and linearity of PRUD, a pre-calibrated commercial transducer (Panametrics-NDT V303, 1 MHz, Olympus) is placed perpendicularly under the prism with a 1 cm interval between the transducer surface and the bottom of prism. The interval was filled with DI water. The transducer, driven by the pulse receiver (5072PR Pulse Receiver, Olympus), can generate acoustic pressure waves striking on the prism with pressure from 500 Pa to 48 kPa. The detected signal (black points) demonstrated a good linearity with the ultrasonic pressure, as shown in Fig. 4(b). The measured noise equivalent pressure (NEP) is about 1.7 kPa.

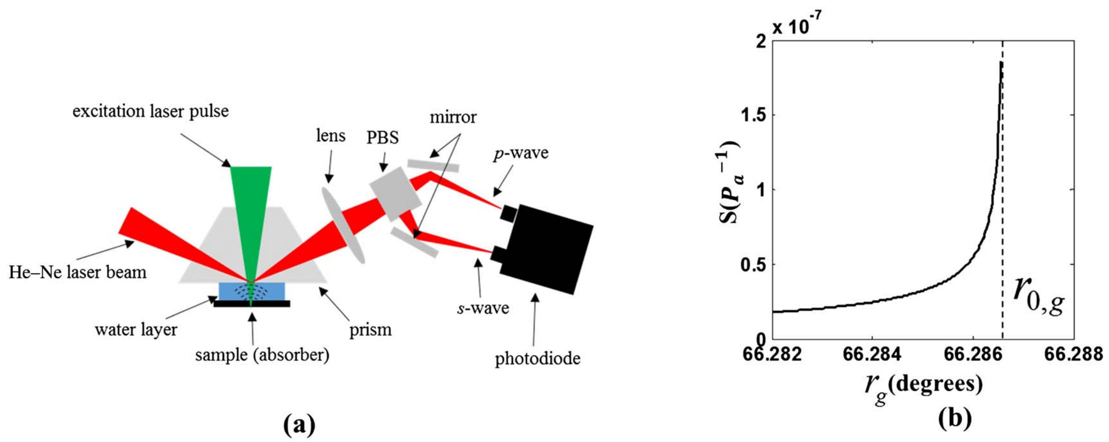

Fig. 2. Schematic of the PRUD. (a) PRUD head and (b) sensitivity versus incident angle.

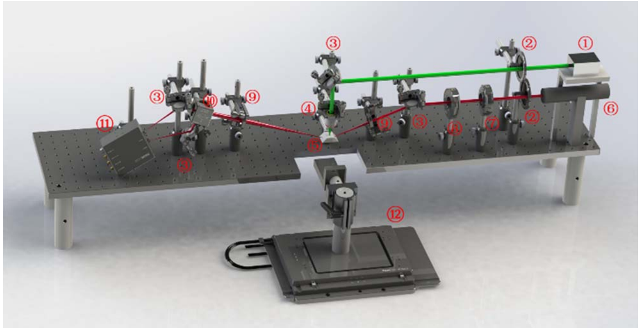

Fig. 3. Overall PRUD system design. ① pulsed excitation laser, ② neutral-density filter, ③ mirror, ④ objective lens, ⑤ trapezoid prism, ⑥ continuous-wave laser, ⑦ polarizer, ⑧ quarter-wave plate, ⑨ lens, ⑩ polarization beam splitter, ⑪ balanced detector, and ⑫ electrical displacement platform.

Next, we performed a photoacoustic microscopy *in vivo* imaging on this PRUD setup. Owing to the transparent prism, we can easily shine the excitation light from the top to perform the reflection mode imaging, where the target was put under the prism. This epi-illumination and detection configuration is crucial for *in vivo* study. We used the same laser as the bandwidth test, but slightly focused it through an objective lens (NA = 0.1). The lateral resolution was determined by the optical focusing, which was measured to be about 14 μm by imaging a 10 μm tungsten wire. We used a Kunming mouse for our *in vivo* experiments. The mouse was first anesthetized by an intraperitoneal injection of chloral hydrate solution at 0.1 mg/g; then we fixed it on the electrical translational stage (MS-2000, Applied Scientific Instrumentation) and raster scanned the ear (about 200 μm thick) with 600 nJ/pulse and 6 μm step size without data averaging. The animal's body temperature was maintained with an infrared lamp. All research complied with protocols approved by the Institutional Animal Care and the Use Committee of Peking University. The mouse recovered to its normal behavior condition after the experiments, and there was no observable damage to its ear. Figure 5 shows the maximum amplitude projected image and its 3D reconstruction of the mouse ear. A 3D animation visualization is also available online (see Visualization 1). The image acquisition time was 15 min.

In summary, we developed a broadband and sensitive ultrasonic detector, PRUD, which relied on the polarization-dependent optical reflection. Unlike works in previous literatures, the PRUD detects the intensity difference between the two polarization states by using a balanced detector. The NEP is substantially improved from the scale of 1 bar to 1 kPa. Compared with traditional photoacoustic microscopy that uses a piezo-electric-material-based transducer, the PRUD has a much broader bandwidth of over 100 MHz with a flat response, and the effective size of the PRUD detector is also much smaller. Moreover, the transparent tapered prism without any coating is very convenient for reflection mode photoacoustic imaging. We demonstrated its superior performance by an *in vivo* PAM imaging of a mouse ear. The NEP and bandwidth of this system are primarily limited by the electrical noise and bandwidth of the balanced detector, which still can be improved in future work. Compared with other current pure-optical ultrasonic detectors, we believe the PRUD is one of the simplest one. Thus, this PRUD would have a great potential to be used in both ultrasound and photoacoustic imaging.

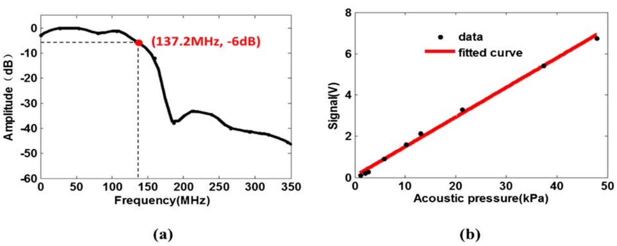

Fig. 4. Characterization of the PRUD. (a) Frequency response and (b) linearity characterization.

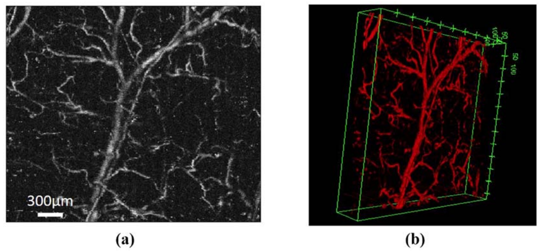

Fig. 5. PA image of a mouse ear using PRUD. (a) Maximum amplitude projected image and (b) screenshot of the 3D visualization (see Visualization 1).

Funding. Ministry of Education of the People's Republic of China (MOE) (20130001110035); National Key Instrumentation Development Project (2011YQ030114, 2013YQ030651); National Natural Science Foundation of China (NSFC) (81421004).

Acknowledgment. The authors thank Dr. Fei Xing and Prof. Xiaocong Yuan's for helping with the system setup. They also thank Dr. Zhaolong Chen and Prof. Zhongfan Liu for providing the graphene sheet.

REFERENCES

1. S. Zackrisson, S. M. W. Y. van de Ven, and S. S. Gambhir, Cancer Res. **74**, 979 (2014).
2. P. Beard, Interface Focus **1**, 602 (2011).
3. C. Li and L. V. Wang, Phys. Med. Biol. **54**, R97 (2009).
4. L. V. Wang and S. Hu, Science **335**, 1458 (2012).
5. G. Paltauf, R. Nuster, M. Haltmeier, and P. Burgholzer, Appl. Opt. **46**, 3352 (2007).
6. S. A. Carp, A. Guerra Iii, and S. Q. Duque, Jr., and V. Venugopalan, Appl. Phys. Lett. **85**, 5772 (2004).
7. J. Horstmann, H. Spahr, C. Buj, M. Munter, and R. Brinkmann, Phys. Med. Biol. **60**, 4045 (2015).
8. E. Zhang, J. Laufer, and P. Beard, Appl. Opt. **47**, 561 (2008).
9. Z. Xie, S.-L. Chen, T. Ling, L. J. Guo, P. L. Carson, and X. Wang, Opt. Express **19**, 9027 (2011).
10. B. Dong, H. Li, Z. Zhang, K. Zhang, S. Chen, C. Sun, and H. F. Zhang, Optica **2**, 169 (2015).
11. Y. Wang, C. Li, and R. K. Wang, Opt. Lett. **36**, 3975 (2011).
12. T. X. Wang, R. Cao, B. Ning, A. J. Dixon, J. A. Hossack, A. L. Klibanov, Q. F. Zhou, A. Wang, and S. Hu, Appl. Phys. Lett. **107**, 153702 (2015).
13. G. Paltauf, H. Schmidt-Kloiber, and H. Guss, Appl. Phys. Lett. **69**, 1526 (1996).
14. J. Niewisch, Sens. Actuators A **25**, 213 (1990).
15. G. Paltauf and H. Schmidt-Kloiber, J. Appl. Phys. **82**, 1525 (1997).
16. F. Xing, G.-X. Meng, Q. Zhang, L.-T. Pan, P. Wang, Z.-B. Liu, W.-S. Jiang, Y. S. Chen, and J.-G. Tian, Nano Lett. **14**, 3563 (2014).